Draft version August 17, 2021
Typeset using LaTeX **twocolumn** style in AASTeX631

Utilizing Spectral Energy Distributions to Classify Circumstellar Shells

Megan G. Frank[1, 2]

[1] *Austin College*
[2] *National Radio Astronomy Observatory*

ABSTRACT

Asymptotic Giant Branch stars can harbor different types of masers depending on properties of their shells. Thicker shells tend to produce OH masers while thinner shells can produce SiO masers. IRAS Low-Resolution Spectra (LRS) are helpful tools for classifying circumstellar shells and determining the thickness, as well as other properties, of the shells. However, there are not very many of them, certainly not enough of them to classify sources across the entire sky. This project aims to take sources from a 2019 VLA OH Maser survey and utilize the shapes of their Spectral Energy Distributions to classify the shells rather than use their LRS.

Keywords: Asymptotic giant branch stars (2100), Spectral energy distribution (2129), Infrared photometry (792), Circumstellar shells (242), Circumstellar masers (240)

1. INTRODUCTION

In 2019, there was a VLA OH Maser Survey conducted to locate Asymptotic Giant Branch (AGB) stars that could possibly harbor OH Masers. AGB stars are stars that have recently completed their time as giant stars, and are working their way towards becoming planetary nebulae. As giants, they experience mass loss that eventually collects around the star to create a shell. If the shell is thick enough, it is possible for the star to harbor an OH Maser.

In order to determine the likelihood of a star harboring an OH maser, it is useful to classify the circumstellar shell. One way to classify these shells is to use IRAS Low-Resolution Spectra (LRS). LRS are spectra taken by the IRAS Low-Resolution Spectrometer. The sources for these spectra were selected based on three criteria: they must have had at least two complete spectra taken, the averaged spectrum must have passed a visual inspection to determine if the spectrum was confused, and the source of the spectrum must have been included in the IRAS Point-Source Catalogue (Olnon et al. 1986).

There are several types of LRS: C, S, F, P, A, E, H, U, and I-type. C-type LRS indicate Carbon Stars and have an 11 μm SiC emission. S-type LRS indicate stellar blackbody sources that have stars with spectral types earlier than M5. F-type LRS are flatter than blackbodies and are expected to be either carbon stars or M-type stars that have a small amount of circumstellar dust. P-type sources have an 11.3 μm emission feature from PAH molecules. These LRS can sometimes be mixed with A-type sources, with A-type sources showcasing a silicate absorption feature at 9.7 μm. That same silicate feature is shown as an emission feature in E-type sources. H-type sources indicate planetary nebulae, and have either silicate absorption features or a PAH emission feature at 11.3 μm. U-type sources are unusual sources with features that are present due to unknown origins. Finally, I-type sources indicate incomplete or noisy spectra (Volk & Cohen 1989). See Figure 1 for examples of each LRS type.

For the purposes of this project, only the E, A, P, and C-type sources will be identified individually due to their potential for harboring masers. E-types have thinner shells that could harbor SiO masers and A-types have thicker shells that could harbor OH masers. Carbon stars, however, could have different properties of their shells compared to OH maser shells. This makes them interesting to study. P-types are included in the list since their LRS can be confused with A-type LRS. This confusion can be seen in Figure 1d (P-type LRS) and 1e (A-type LRS). Both of these LRS have dips located in around the same spot, which can lead to some difficulty in distinguishing the two spectral types.

LRS are great tools to use to classify circumstellar shells. However,due to the selection criteria as discussed above, there are a limited number of LRS. This makes it difficult to classify circumstellar shells across the entire sky. So, instead of using LRS, this project aims to

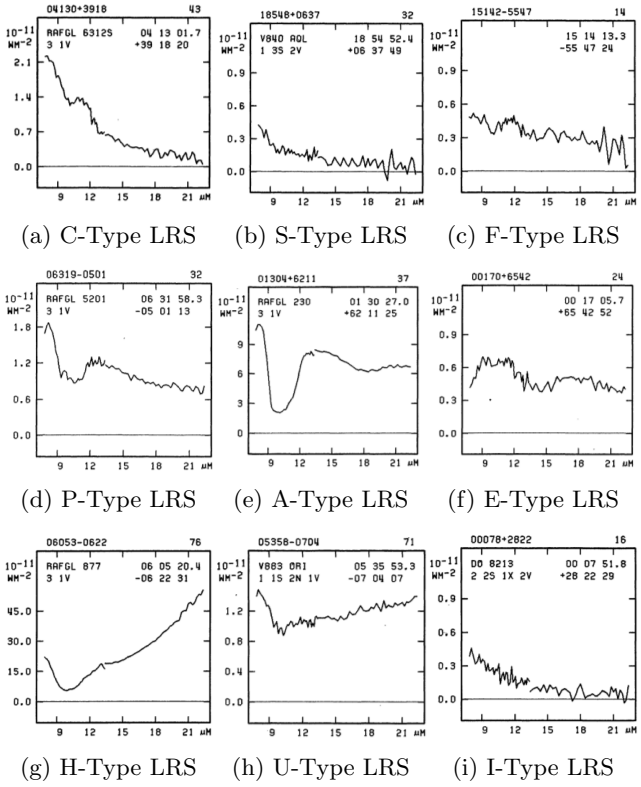

(a) C-Type LRS (b) S-Type LRS (c) F-Type LRS

(d) P-Type LRS (e) A-Type LRS (f) E-Type LRS

(g) H-Type LRS (h) U-Type LRS (i) I-Type LRS

Figure 1: Examples of the different types of LRS. All LRS have wavelength in μm on the x-axis and intensity in Wm^{-2} on the y-axis (Olnon et al. 1986).

utilize Spectral Energy Distributions (SEDs) to classify circumstellar shells.

The paper proceeds as follows. Section 2. Data describes where the data comes from. Section 3. Methods describes the methods used to create and sort SEDs as well as plotting infrared diagrams. Section 4. Results showcases the results. Section 5. Discussion highlights certain aspects of the results while also discussing potential improvements. Section 6. Conclusion provides a summary of the project. Finally, section 7. Future Work gives insight into projects and improvements that should occur as a result of this project.

2. DATA

The original sample for this project comes from the selection of AKARI survey targets choosen for the 2019 VLA OH Maser Survey as described above. The following infrared all-sky surveys were also used: 2MASS, WISE All-SKY, IRAS, and AKARI. Additionally, the IRAS LRS database was used.

3. METHODS

The first step in this process was to cross-match the sources from the 2019 VLA OH Maser Survey with the IRAS Point-Source catalogue. This was done to allow for easier cross-matching with the LRS catalogue, as the object names in the IRAS Point-Source Catalogue are the same as the object names in the LRS catalogue, which we then cross-matched to. The list was then cross-matched separately with the 2MASS Point-Source Catalogue and the WISE All-SKY Source catalogue. Then, both of those list were cross-matched to each other. That final list was then cross-matched with the AKARI catalogue. After the cross-matching was completed, there were 697 sources remaining. This includes 452 E-type sources, 48 A-type sources, 15 P-type sources, 16 C-type sources, and 166 sources that were attributed to the LRS that are not the primary focus of this project.

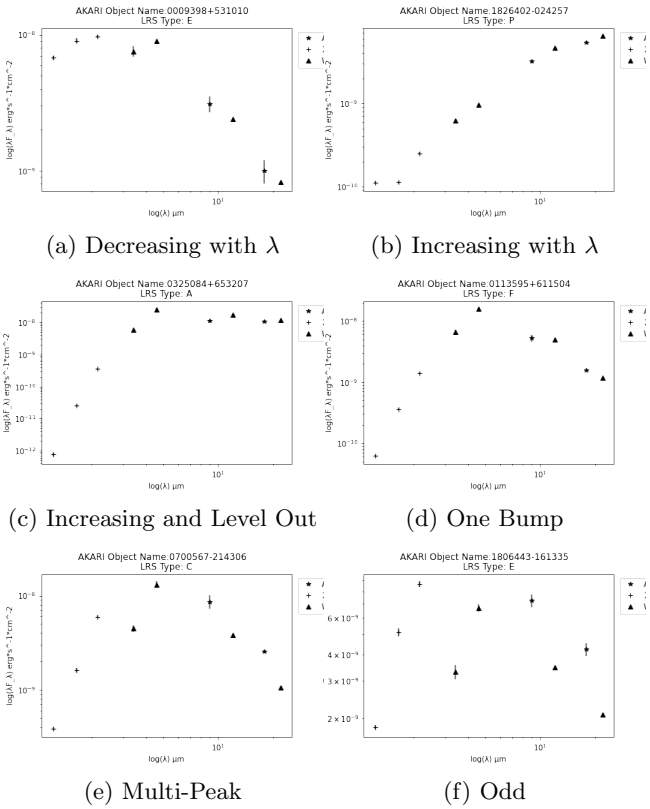

(a) Decreasing with λ (b) Increasing with λ

(c) Increasing and Level Out (d) One Bump

(e) Multi-Peak (f) Odd

Figure 2: Examples of sorted SEDs. Wavelength in μm is on the x-axis and flux density in ergs*s^{-1}*cm^{-2}. The plus points are from 2MASS, the stars are from AKARI, and the triangles are from WISE All-SKY.

SEDs were then created and sorted for all 697 sources. The sorting was done by hand based on the shapes of each SED. Six shape categories were created: decreasing with wavelength, increasing with wavelength, increasing and leveling out, one bump, multi-peak, and odd. The SEDs in the odd category were SEDs that could not be

placed in any other category. See Figure 2 for examples of SEDs in each category. All of the sorted SEDs can be found in a Google folder at this link.

After the SEDs were sorted, five infrared diagrams were created. We created a 2MASS color-color diagram, 2MASS color-magnitude diagram, IRAS color-color diagram, AKARI color-color diagram, and the AKARI/IRAS color-color diagram from Koopman et al. (2011).

4. RESULTS

On the infrared diagrams, the LRS-type determined the color of the markers and the SED shape determined the shape of the markers. A legend that is applicable for all of the infrared diagrams is found in Figure 3.

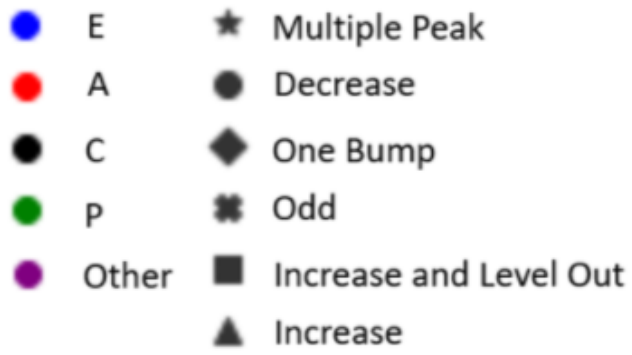

Figure 3: Legend for all of the infrared diagrams.

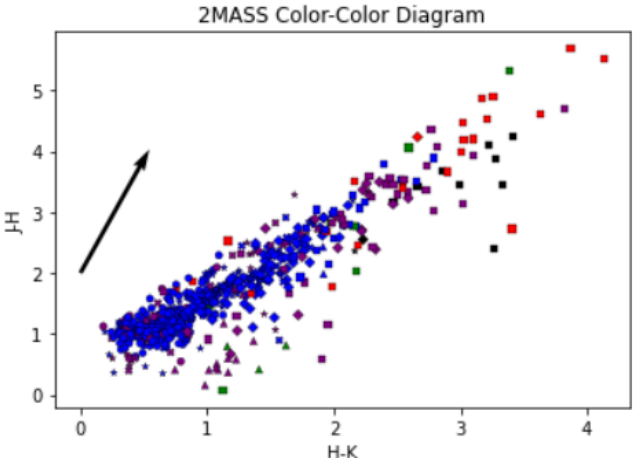

Figure 4: 2MASS Color-Color Diagram. The H-K color is on the x-axis and the J-H color is on the y-axis. A reddening vector is shown on the left side of the diagram. See Figure 3 for the legend.

The 2MASS color-color diagram is shown in Figure 4, with the H-K color on the x-axis and the J-H color on the y-axis. On the diagram, the blue, E-type sources all accumulate in the bottom left corner of the diagram. There is also a reddening vector on the left side of the diagram.

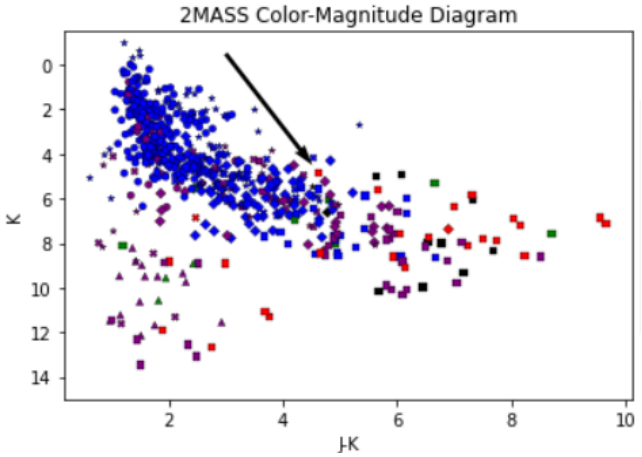

Figure 5: 2MASS Color-Magnitude Diagram. The J-K color is on the x-axis and the K-magnitude is on the y-axis. A reddening vector is shown on the top of the diagram. See Figure 3 for the legend.

Figure 5 shows the 2MASS color-magnitude diagram. This diagram has the J-K color on the x-axis and the K magnitude on the y-axis with the brightest sources towards the top of the diagram. This diagram is similar to the 2MASS color-color diagram in that it has the blue E-type sources grouped together, this time in the upper left corner. This diagram also has a reddening vector, this time on the top of the diagram.

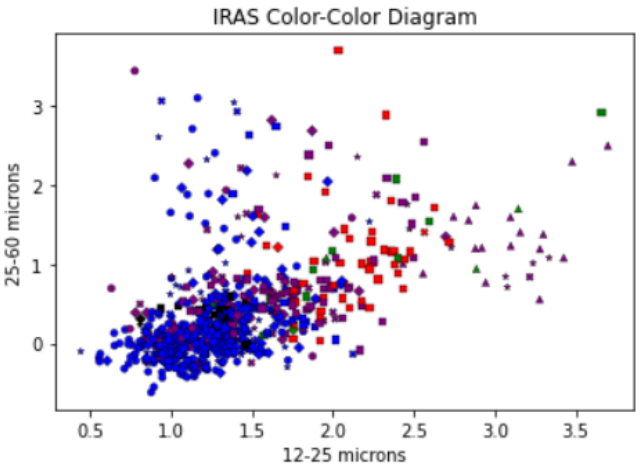

Figure 6: IRAS Color-Color Diagram. The 12-25 μm color is on the x-axis and the 25-60 μm color is on the y-axis. See Figure 3 for the legend.

The IRAS color-color diagram is shown in Figure 6. This figure has the 12-25 μm color on the x-axis and the 25-60 μm color on the y-axis. This figure also has most of the E-type sources grouped in the bottom left corner.

Figure 7 shows the AKARI color-color diagram which has the 9-18 μm color on the x-axis and the 18-90 μm color on the y-axis. This diagram also has the E-type sources grouped in the bottom left corner.

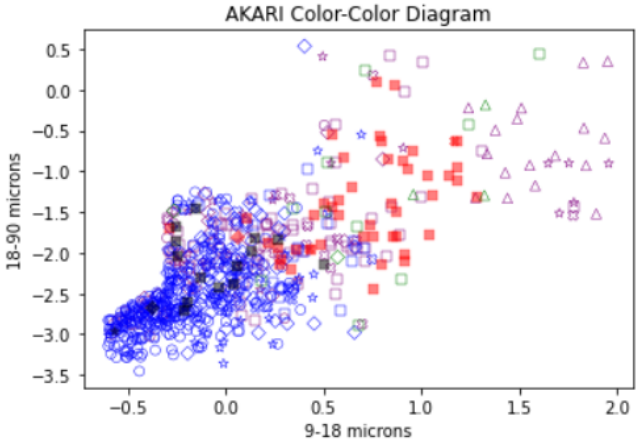

Figure 7: AKARI Color-Color Diagram. The 9-18 μm color is on the x-axis and the 18-90 μm color is on the y-axis. See Figure 3 for the legend.

The Koopman et al. (2011) color-color diagram in Figure 8 uses colors from both the IRAS catalogue and the AKARI catalogue. The IRAS 12-25 μm color is on the x-axis and the AKARI 9-18 μm color is on the y-axis.

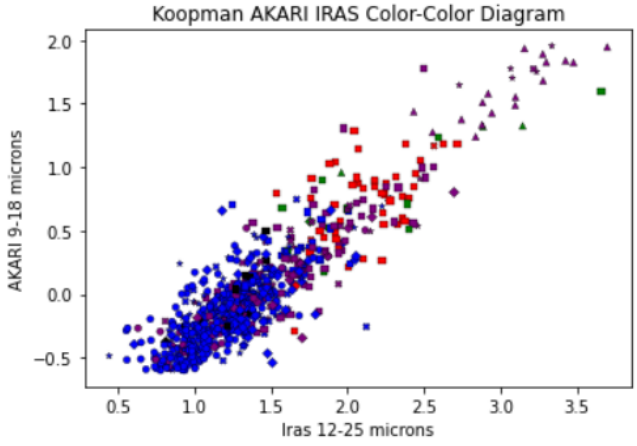

Figure 8: Koopman et al. (2011) Color-Color Diagram. This diagram has the IRAS 12-25 μm color along the x-axis and the 9-18 μm color on the y-axis. See Figure 3 for the legend.

5. DISCUSSION

The infrared diagrams all have a pretty distinct feature: the E-type sources are all grouped together. Additionally, the A-type sources are grouped together and the C-type sources are grouped together. In order to see the latter feature more clearly, Figure 9 is shown, which is the AKARI color-color diagram without the E-type sources. The colors and shapes of the markers still matches with the legend in Figure 3 (See section 4. Results).

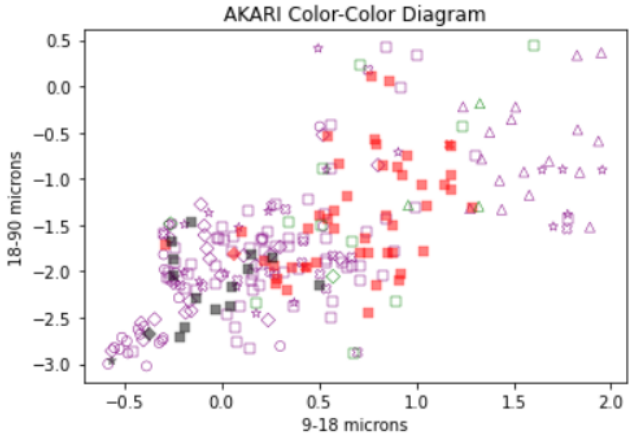

Figure 9: AKARI Color-Color Diagram without the blue, E-type sources. The 9-18 μm color is on the x-axis and the 18-90 μm color is on the y-axis. See Figure 3 for the legend.

In Figure 9, it becomes easier to see the distribution of the not-E-type sources. The C-types seem to group together near the bottom left of the diagram, while the A-type sources seem to group together in the middle of the diagram. There is very little crossover between the two groups.

Additionally, most, if not all, of the C-type and A-type sources have SEDs that increase and level-out. Looking back at the E-types, we see that those SEDs are mostly in the decreasing category. Very few other sources have decreasing SEDs.

Taking all of this information into account, LRS types are not needed to classify source shells if an SED can be produced for said shells. If a shell has an SED that is decreasing, one can say that it has the characteristics of an E-type LRS. If the SED is increasing and leveling out, it can be plotted on a color-color diagram to determine whether it is a C-type or A-type source.

There are two main sources of error in this project. One would come from sorting the SEDs by hand. A more standardized way of sorting them, possibly utilizing coding methods, would help to eliminate some of that error. The larger of the two errors comes from

the WISE ALL-Sky W1 and W2 bands. In these two bands, there is a greater potential for error due to saturation in really bright sources. As the sources that were looked at may harbor OH Masers, it is safe to say that these sources are quite bright. This is mostly an issue in AllWISE, but it is something to be aware of since the W1 and W2 bands in WISE All-SKY are only somewhat more accurate for bright sources. See the AllWISE Cautionary Notes for details. Having this issue with the W1 and W2 band could lead to some errors with sorting the SEDs properly.

6. CONCLUSION

This project started with 1355 sources from the 2019 VLA OH Maser Survey. After cross-matching with IRAS, 2MASS, WISE All-SKY, AKARI, and the IRAS LRS database, 697 sources remained in the sample. From these 697 sources, SEDs were made. These SEDs were hand-sorted into six categories based on shape. After this, the sources were plotted on five different color-color diagrams with LRS type indicating marker color and SED shape indicating marker shape. These color-color diagrams show that the sources are grouped by LRS type. The E-types have SEDs that are mostly decreasing, and the C-types and A-types have SEDs that are increasing and leveling out. By looking at the SEDs of these sources and plotting the sources on a color-color diagram, one can determine properties and classify the circumstellar shells of evolved stars without the use of LRS.

7. FUTURE WORK

Future work should strive to find a more standardized way of sorting the SEDs to eliminate errors caused by sorting them by hand. Once this has been done, it will be reasonable to apply this method to sources that do not have an LRS classification so that they may be classified.

There should also be work done to see if a more "complete" SED would prove more useful for classifying sources. By utilizing more all-sky surveys in other bands, one could achieve this. However, since the sources in this survey were selected in hopes of harboring OH masers, it would be best to only use wavelengths starting at near-infrared and continuing through the radio end of the electromagnetic spectrum.

It may also be useful to check if this method holds true with the other LRS types that were not included in the focus of this project (i.e. the S, F, H, U, and I types).

Thank you to all of those who have assisted me with this project, be it for help on the project itself or support along the way. This is including but not limited to my NRAO mentors Mark Claussen and Lorant Sjouwerman, the Austin College Physics Department, and my roommates and friends.

REFERENCES

Koopman, K., Sjouwerman, L., & Claussen, M. 2011, in American Astronomical Society Meeting Abstracts, Vol. 217, American Astronomical Society Meeting Abstracts #217, 154.05

Olnon, F. M., Raimond, E., Neugebauer, G., et al. 1986, A&AS, 65, 607

Volk, K., & Cohen, M. 1989, AJ, 98, 931,

doi: 10.1086/115188